

Sidelobe Control for Bistatic SAR Imaging

Viet T. Vu^{ID}, *Senior Member, IEEE*, and Mats I. Pettersson^{ID}, *Senior Member, IEEE*

Abstract—This letter presents coherent and incoherent nonlinear apodization methods for bistatic synthetic aperture radar (SAR) imaging. The methods are developed on the principle of nonlinear apodization for monostatic SAR imaging and a $\omega - k$ relationship representing the bistatic region of support. This relationship plays an important role in designing 2-D windows for the apodization methods. The simulation results show that the presented apodization methods work efficiently with bistatic SAR imaging. In the experiment with a coherent dual apodization (CDA) method presented in this letter, the sidelobe attenuates very fast, and the peak sidelobe is reduced about 16 dB, while the resolutions in azimuth and range are maintained.

Index Terms— $\omega - k$, apodization, bistatic, resolution, sidelobe, synthetic aperture radar (SAR).

I. INTRODUCTION

BISTATIC synthetic aperture radar (SAR) refers to SAR systems with separated transmitter and receiver. This separation brings a number of advantages for bistatic SAR in vulnerability reduction, object classification, jamming resistance, and so forth. However, the advantages of bistatic SAR accompany with some invariably challenges, such as synchronization and signal processing. This partly explains why there are a large number of researches on bistatic SAR synchronization and bistatic SAR signal processing [1]–[4]. Besides this, the practical issues for bistatic SAR, such as sidelobe control, autofocus, and image quality measurements, are also very important.

In an SAR scene, where objects with large radar cross sections (RCSs), such as buildings, ships, and power lines, are present, controlling sidelobe in SAR imaging is necessary; otherwise, the sidelobes of these objects can widely spread and obscure the surrounding objects. Sidelobe control by apodization methods allows revealing the obscured objects. A summary of linear and nonlinear apodization methods for monostatic SAR can be found in [5] and [6]. It is common knowledge that linear apodization refers to the sidelobe control methods that weigh the region of support of an SAR image, i.e., the 2-D Fourier transform of SAR image, with windows, such as Hamming, Hanning, and Blackman. The linear apodization methods help to suppress the sidelobe, but the expense for this suppression is the broadening of the mainlobe. Nonlinear apodization is a combination of linear apodization methods with nonlinear operators. One typical

nonlinear operator is a selection of minimum magnitudes among the original (unweighted) SAR image and the weighted SAR images obtained with the linear apodization methods on a pixel-by-pixel basis. By this, the nonlinear apodization methods can suppress sidelobes without broadening the mainlobe. The critical issue for a linear or a nonlinear apodization method is how to design the 2-D windows for weighting. For monostatic SAR, designing a window is simply based on the monostatic $\omega - k$ relationship [7] representing the region of support of monostatic SAR image. For bistatic SAR, a bistatic $\omega - k$ relationship is a prerequisite for designing 2-D windows. A new bistatic $\omega - k$ relationship has been introduced recently in [8] opening the opportunities to develop the apodization methods for controlling sidelobe in bistatic SAR imaging.

In this letter, we present coherent and incoherent nonlinear apodization methods for bistatic SAR imaging based on the principle of nonlinear apodization for monostatic SAR imaging and the bistatic $\omega - k$ relationship derived in [8].

The rest of this letter is organized as follows. Section II reviews the apodization methods for monostatic SAR imaging. Section III presents the apodization methods for bistatic SAR imaging. The bistatic $\omega - k$ relationship and designing 2-D windows based on this relationship are provided in detail. Section IV gives some simulation results to examine the presented apodization methods. Section V gives the concluding remarks.

II. SIDELOBE CONTROL FOR MONOSTATIC SAR IMAGING

The currently used methods for sidelobe control in SAR imaging are categorized by linear and nonlinear apodization methods. A nonlinear apodization is a combination of linear apodization and nonlinear operators. Linear apodization can simply be implemented by filtering the region of support, i.e., 2-D Fourier transform, of SAR images with 2-D windows, such as rectangle, Hamming, Hanning, and Blackman, whereas a nonlinear operator can be a selection of minimum magnitude. Designing the 2-D windows affects significantly the performance of apodization and must be based on the $\omega - k$ relationship for monostatic SAR representing the region of support

$$\omega = \frac{c_0}{2} \sqrt{k_\xi^2 + k_\rho^2} \quad (1)$$

where k_ξ and k_ρ are azimuth wavenumber and range wavenumber, respectively, ω is angular radar signal frequency, and c_0 is the speed of wave propagation. This relationship is well-known and is the basis of the Stolt interpolation, which is the kernel of the range migration or the $\omega - k$ algorithm [7].

Manuscript received May 28, 2021; revised July 5, 2021; accepted July 19, 2021. (Corresponding author: Viet T. Vu.)

The authors are with the Blekinge Institute of Technology, 37179 Karlskrona, Sweden (e-mail: viet.thuy.vu@bth.se).

Color versions of one or more figures in this letter are available at <https://doi.org/10.1109/LGRS.2021.3099174>.

Digital Object Identifier 10.1109/LGRS.2021.3099174

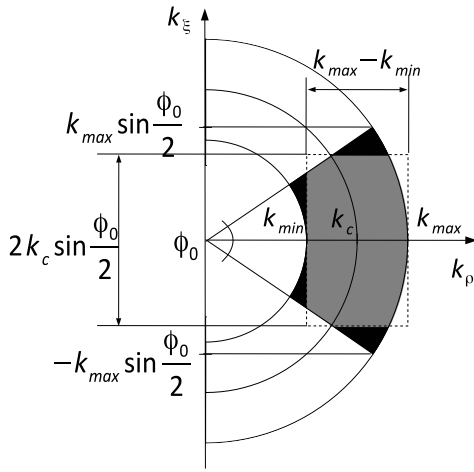


Fig. 1. Region of support obtained with the 2-D Fourier transform a monostatic SAR image (black), 2-D rectangle window (fine-dashed-line), and weighted region of support (gray area).

Equation (1) is a function of circle having center at $(k_\xi = 0, k_\rho = 0)$ and radius given by $2\omega/c_0$, as illustrated in Fig. 1. For linear apodization, the 2-D windows can be defined inside the $2k_c \sin(\phi_0/2) \times (k_{\max} - k_{\min})$ rectangle, where ϕ_0 is the integration angle.

A convenient way to design the 2-D windows is to use a 2-D cosine-on-pedestal function

$$W(k_\xi, k_\rho) = \left[0.5 + \epsilon_\rho \cos\left(\frac{2\pi(k_\rho - k_c)}{k_{\max} - k_{\min}}\right) \right] \times \left[0.5 + \epsilon_\xi \cos\left(\frac{2\pi k_\xi}{2k_c \sin(\phi_0/2)}\right) \right] \quad (2)$$

where ϵ_ξ and ϵ_ρ are weighting factors, and $k_c = (k_{\max} - k_{\min})/2$. For $\epsilon_\xi = \epsilon_\rho = 0$, we get a 2-D rectangular window, while, for $\epsilon_\xi = \epsilon_\rho = 0.5$, we get a 2-D Hanning window. To get a 2-D Hamming window, we can set $\epsilon_\xi = \epsilon_\rho = 0.426$ followed by a normalization step $(0.54/0.5)$. Hence, using 2-D cosine-on-pedestal function for apodization simplifies an optimization between sidelobe suppression and losses in spatial resolutions.

Assume that weighting the 2-D Fourier transform of an SAR image \mathfrak{I}_0 using different 2-D window results in a set of weighted images $[\mathfrak{I}_1, \mathfrak{I}_2, \dots, \mathfrak{I}_N]$. The images, both unweighted and weighted, are normalized so that they have the same peak magnitudes. For convenience, we can normalize $\max\{|\mathfrak{I}_i|\} = 1$ the image. A nonlinear apodized image can be obtained with the selection of the minimum magnitudes on a pixel-by-pixel basis

$$|\mathfrak{I}(\xi, \rho)| = \min\{|\mathfrak{I}_0(\xi, \rho)|, |\mathfrak{I}_1(\xi, \rho)|, \dots, |\mathfrak{I}_N(\xi, \rho)|\}. \quad (3)$$

Because this nonlinear operator considers only the magnitudes and ignores the phases of the SAR image, this kind of apodization is seen to be incoherent. If two images are taken into account in the nonlinear operator (3), i.e., \mathfrak{I}_0 and $\mathfrak{I}_{i \neq 0}$, an incoherent dual apodization (IDA) will be obtained. Incoherent triple apodization or incoherent multiple apodizations

can be obtained with three or more windows to be considered in the nonlinear operator (3).

To maintain the phase information of SAR image, the pair of unweighted and weighted SAR images can be analyzed in real and imaginary parts. The nonlinear operator can be performed separately on both real and imaginary parts on a pixel-by-pixel basis so that

$$\mathcal{O}[\mathfrak{I}] = \begin{cases} 0 & \mathcal{O}[\mathfrak{I}_0]\mathcal{O}[\mathfrak{I}_i] < 0 \\ \text{sign}\{\mathcal{O}[\mathfrak{I}_0]\} & \\ \times \min\{|\mathcal{O}[\mathfrak{I}_0]|, |\mathcal{O}[\mathfrak{I}_i]|\} & \text{else} \end{cases} \quad (4)$$

where \mathcal{O} refers to Re and Im operators. The assigning zero is interpreted as an intermediate weighting function between unweighted and weighted. Due to a separated consideration of the real and imaginary parts of SAR images, this procedure is named coherent or complex dual apodization (CDA).

As mentioned, weighting the region of support with a 2-D window (2) always accompanies losses in resolution. For the narrowband and narrowbeam cases, the coupling between azimuth and range frequencies is small. There is almost no loss in both azimuth and range resolutions if weighting the region of support with a 2-D rectangular window. It is possible to find a window that optimizes the acceptable losses in resolution and the expected level of sidelobe suppression. For ultrawideband (UWB) SAR, the losses in resolutions are significant, and these losses occur even if weighting the region of support with a 2-D rectangular window [9]. As illustrated in Fig. 1, the region of support (black area) is narrowed (gray area) by the 2-D rectangular window. Therefore, linear apodization is said to be inefficient and not recommended for monostatic UWB SAR imaging. Herein, the inefficiency shows by either a high loss in resolution or the insignificant sidelobe suppression. For this reason, nonlinear apodization is only the possibility for monostatic UWB SAR imaging. This conclusion is also applied to bistatic UWB SAR imaging.

III. SIDELobe CONTROL FOR BISTATIC SAR IMAGING

Sidelobe control for bistatic SAR imaging is recommended based on nonlinear apodization. Designing the 2-D windows must also be based on an $\omega - k$ relationship for bistatic SAR, whereas the nonlinear operators for monostatic apodization can also be used for the bistatic case without any modification.

A. $\omega - k$ Relationship for Bistatic SAR

The main difference between an $\omega - k$ relationship for bistatic SAR and the one for monostatic SAR is the bistatic factor that is included in the relationship. This factor is a function of the coordinates of the SAR platforms or, in other words, a function of time. As proposed in [8], a general $\omega - k$ relationship for bistatic SAR is given by

$$\omega = \frac{c}{2\chi} \sqrt{k_\xi^2 + k_\rho^2} \quad (5)$$

where χ denotes the bistatic factor and is calculated by

$$\chi = \frac{1}{2} \sqrt{(\sin \alpha_T + \sin \alpha_R)^2 + (\epsilon_T \cos \alpha_T + \epsilon_R \cos \alpha_R)^2}. \quad (6)$$

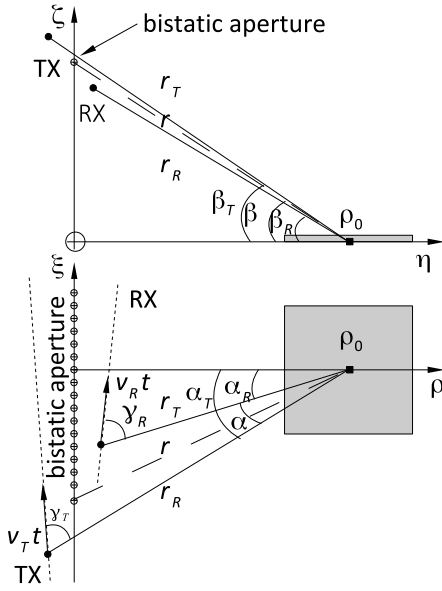


Fig. 2. Bistatic SAR geometry.

The angles $\alpha_{(\cdot)}$ are formed by $\vec{r}_{(\cdot)}$ and $\vec{\rho}_0$, as illustrated in Fig. 2. The ratios ϵ_T and ϵ_R are defined by

$$\epsilon_T = \frac{\cos \beta_T}{\cos \beta} \quad \epsilon_R = \frac{\cos \beta_R}{\cos \beta} \quad (7)$$

where $\beta_{(\cdot)}$ are the angles formed by $\vec{r}_{(\cdot)}$ and the ground plane, and θ is the angle formed by \vec{r} and the ground plane. For linear movements of SAR platforms, the values of $\alpha_{(\cdot)}$, $\beta_{(\cdot)}$, and $\vec{r}_{(\cdot)}$ are given by the relative positions of the platforms and, therefore, vary with respect to the positions of the platforms.

The function given in (5) is a function of the arch, but the arch border cannot be expressed analytically since χ varies complicatedly with time. This factor is calculated from the angles $\alpha_{(\cdot)}$ and $\beta_{(\cdot)}$, and these angles change with respect to the position of the transmitter and receiver during the measurement time. Hence, χ is a function time t or $\chi(t)$ and not a constant like the monostatic case. Fig. 3 shows an illustration of the region of support for the bistatic case.

Assume that the sampling frequency is the Nyquist frequency. Based on Fig. 3, we can derive the limit of k_ρ when $k_\xi = 0$ by

$$\frac{4\pi v_{\min}}{c_0} \chi(t_0) \leq k_\rho \leq \frac{4\pi v_{\max}}{c_0} \chi(t_0) \quad (8)$$

where v_{\max} and v_{\min} are the maximum and minimum radar frequencies, respectively. The time $t = t_0$ corresponds to the bistatic coordinate that $k_\xi = 0$, i.e.,

$$\chi_\xi(t_0) = \frac{1}{2} [\sin(\alpha_T(t_0)) + \sin(\alpha_R(t_0))] = 0. \quad (9)$$

The limit of k_ξ can also be derived from Fig. 3 by

$$-\frac{4\pi v_{\max}}{c_0} \chi(t_l) \sin \phi_l \leq k_\xi \leq \frac{4\pi v_{\max}}{c_0} \chi(t_u) \sin \phi_u \quad (10)$$

where $t = t_l$ and ϕ_l are the time and the angle corresponding to the initial position of the bistatic aperture, whereas $t = t_u$

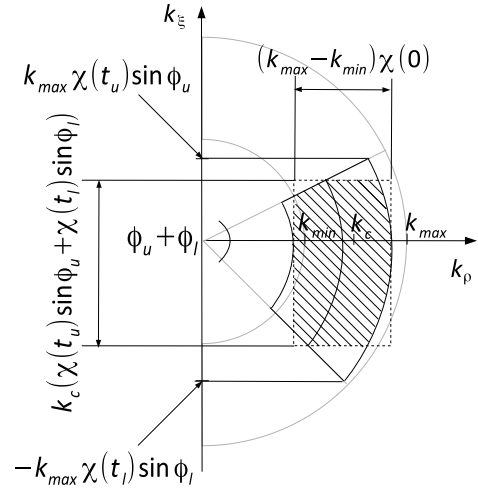


Fig. 3. Region of support obtained with the 2-D Fourier transform a bistatic SAR image (black solid curve), 2-D rectangle window (fine-dashed-line), and weighted region of support (dashed area).

and ϕ_u are the time and the angle corresponding to the last position of the bistatic aperture.

It should be highlighted that the bistatic integration angle depends also on bistatic geometry and, therefore, is different from the geometrical integration angle.

B. Apodization for Bistatic SAR

With a reference to the linear apodization for the monostatic case, the 2-D windows can be defined inside the $k_c(\chi(t_l) \sin \phi_l + \chi(t_u) \sin \phi_u) \times (k_{\max} - k_{\min})\chi(t = 0)$ rectangle for the bistatic case. If we use a 2-D cosine-on-pedestal function to design the 2-D windows, the function is defined by

$$W(k_\xi, k_\rho) = \left[0.5 + \epsilon_\rho \cos \left(\frac{2\pi [k_\rho - k_c \chi(t_0)]}{(k_{\max} - k_{\min}) \chi(t_0)} \right) \right] \times \left[0.5 + \epsilon_\xi \cos \left(\frac{2\pi k_\xi}{k_c [\chi(t_l) \sin \phi_l + \chi(t_u) \sin \phi_u]} \right) \right]. \quad (11)$$

The 2-D Fourier transform of a bistatic UWB SAR image \mathfrak{S}_0 can be weighted by different 2-D windows by setting different values for ϵ_ρ and ϵ_ξ . A set of weighted images $[\mathfrak{S}_1, \mathfrak{S}_2, \dots, \mathfrak{S}_N]$ is then retrieved after this weighting step. The nonlinear operators (3) and (4) can be used for retrieving a nonlinear apodized image from the unweighted and weighted images.

IV. EXPERIMENTAL RESULTS BASED ON SIMULATIONS

In this section, we provide some simulation results to examine the performance of the proposed nonlinear apodization for bistatic SAR imaging. The SAR image quality assessments, such as spatial resolutions and peak sidelobe ratio, are helpful for evaluations.

TABLE I
SIMULATION PARAMETERS

Parameter	Transmitter	Receiver
Frequency range	22.0 – 82.5 MHz	
Platform speed v_{pl}	129 m/s	43 m/s
Aperture step	0.9375 m	0.3125 m
Flight altitude	3700 m	2000 m
PRF	137 Hz	
Num. aperture position	20480	
Initial coordinates	(-6394, -721)	(-6369, 721)
Last coordinates	(12787, -1558)	(-24, 1558)
Flight headings	-2.5°	7.5°

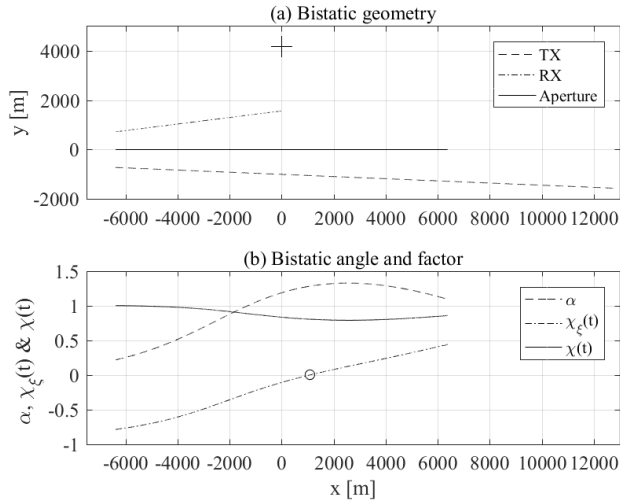


Fig. 4. (a) Arrangement for simulations with the positions of platforms, bistatic aperture and aim point (marked by +) in the (x, y) plane (bistatic geometry). (b) Bistatic angle α , $\chi_\zeta(t)$, and bistatic factor $\chi(t)$. $\chi_\zeta(t_0) = 0$ is marked with the circle.

A. Arrangement

The transmitter is simulated with the parameters of CARABAS-II, while the passive receiver is simulated with the motion parameters of CARABAS-III (speed and altitude). The main parameters for the simulations are summarized in the upper part of Table I. Some supplemental parameters for the simulations are given in the lower part of the table. The flight paths are sketched in Fig. 4(a). The bistatic aperture is formed by the midpoints of the transmitter and receiver coordinates and marked by the black solid line.

The ground scene is simulated with a single point-like scatterer placed in the center of the SAR scene and symmetric with respect to the bistatic aperture. It is marked by the cross in the upper part of Fig. 4(a). The RCS of the scatterer is normalized to one.

With this extreme arrangement, we get a geometrical integration angle of $\phi_0 = 103.5^\circ$. The bistatic integration angle is shown to be $\phi_u + \phi_l = 31.2^\circ + 51.8^\circ = 83.1^\circ$ and significantly narrower than the geometrical integration angle. The bistatic angle varies widely with respect to the platform positions and is up to 75.9° (1.324 radian), as shown in Fig. 4(b). The value of bistatic factor χ estimated for each aperture position is

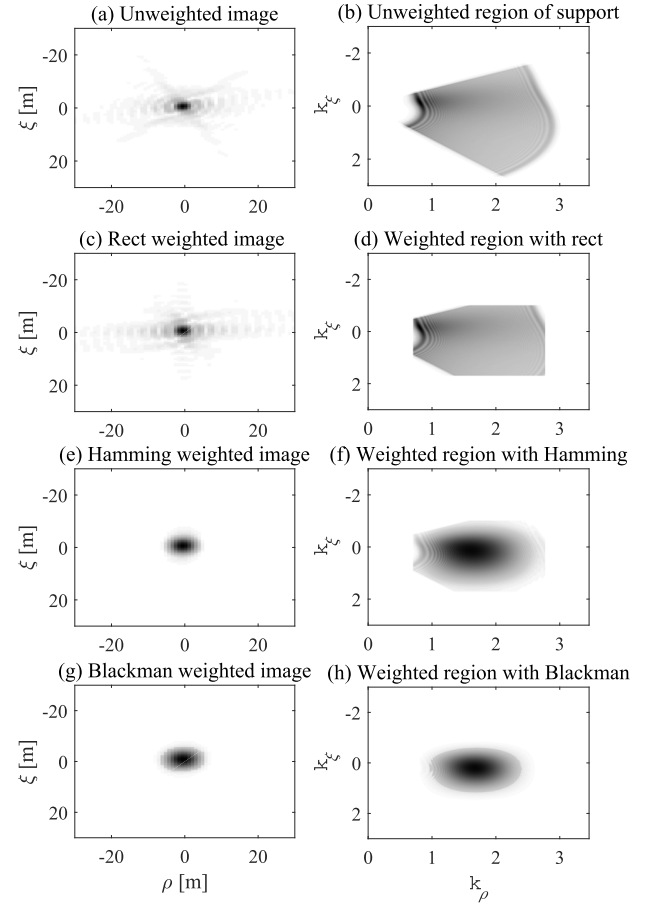


Fig. 5. Weighted/unweighted regions of support and corresponding weighted/unweighted images, (a) and (b) unweighted, (c) and (d) Rect window, (e) and (f) Hamming window, and (g) and (h) Blackman window.

also provided in Fig. 4(b). The factor χ varies complicatedly with respect to the aperture positions, and its values are in the range $[0.7878, 0.9993]$. The extreme values used for designing 2-D windows are $\chi(t_l) = 0.9993$, $\chi(t_u) = 0.8550$, and $\chi(t_0) = 0.8024$.

Fig. 5(a) provides the zoomed-in section of the SAR image in the slant-range plane (ζ, ρ) . The simulated point-like scatterer is well-focused. The 2-D Fourier transform of the SAR image is given in Fig. 5(b) in the form of the arch and matched with the illustration given in Section III.

B. Weighting

Fig. 5(d), (f), and (h) shows the region of support weighted with 2-D rectangular, Hamming, and Blackman windows, whereas Fig. 5(c), (e), and (g) shows the 2-D inverse Fourier transform of the weighted regions of support, i.e., weighted SAR images. Table II summarizes the measured results on the weighted SAR images, including the resolutions in azimuth and range, and peak sidelobe.

For weighting with a 2-D rectangular window, there is no significant effect on sidelobe suppression. The peak sidelobe even increases 1 dB in comparison to that of the original image. The measurements on azimuth and range resolutions

TABLE II
CALCULATED VALUES

	Resolution		Peak sidelobe (in range)
	Azimuth	Range	
Original	2.0 m	2.5 m	−15.0 dB
Rect	2.5 m	2.6 m	−14.0 dB
Hamming	3.2 m	4.0 m	−41.5 dB
Blackman	4.0 m	5.0 m	−55.5 dB
IDA	2.0 m	2.5 m	−17.0 dB
CDA	2.0 m	2.5 m	−31.0 dB

show the losses in the resolutions, in which the loss in the azimuth resolution is 1.25. If we weigh the region of support with the 2-D Hamming window instead of the 2-D rectangular window, a reduction in the sidelobe level is about 26.5 dB (from −15 dB down to −41.5 dB), whereas the loss factor in both azimuth and resolutions is 1.6. We can further suppress the sidelobe level to −55.5 dB with the 2-D Blackman window. However, this 2-D function causes a loss factor in resolutions of 2.0.

C. Nonlinear Apodization

For illustration purposes, we consider here dual apodization based on the original image and the Hamming weighted image. They are the inputs for the nonlinear operators (3) for IDA and (4) for CDA. The nonlinear operators are illustrated with the cuts $\Im_i(\xi = 0, \rho)$ and $\Im(\xi = 0, \rho)$. The cuts are parallel to the range direction and pass through the peak magnitudes of the SAR images.

The performance of the nonlinear operator (3) is shown in Fig. 6(a), in which minimum magnitudes of the unweighted and weighted images are selected to form the apodized image. The image obtained with the IDA is given in Fig. 6(b). Comparing with Fig. 5(a), we can see that the spreading of the sidelobe has been reduced significantly. The measure results on the image reported in Table II show that the peak sidelobe level is −17 dB. The high peak sidelobe is created randomly by the nonlinear operator from the first sidelobe of the original image. This is due to a small number of inputs (dual) and can avoid by increasing the number of inputs of the nonlinear operator, i.e., forming a series of weighted images with the small step of the loss factor in resolutions, or in other words, the high peak sidelobe with IDA can be avoided by incoherent multiple apodizations (more choices for the nonlinear operator). The azimuth and range resolutions are maintained.

Fig. 6(c) shows the performance of the nonlinear operator (4) after combining the real and imaginary parts with $((\text{Re}[\Im])^2 + (\text{Im}[\Im])^2)^{1/2}$. Comparing with Fig. 5(a), we can also see that the spreading of the sidelobe has been reduced significantly. The measure results on the image show a decrease in the peak sidelobe level. The peak sidelobe −31 dB is obtained due to the intermediate weighting function between

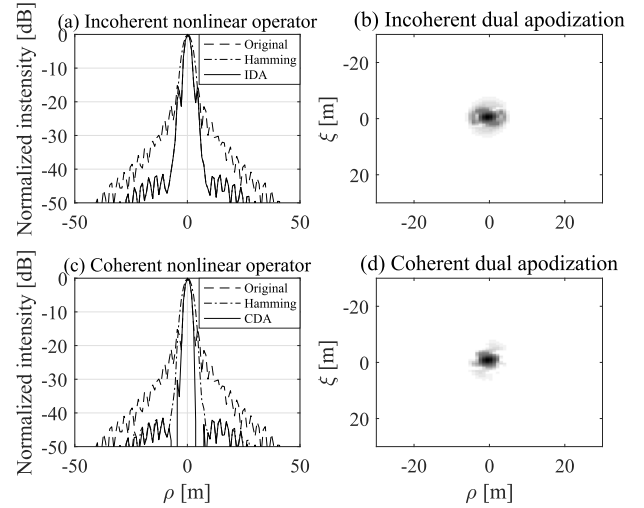


Fig. 6. Results obtained with IDA and CDA. (a) Illustration of operator (3) (incoherent nonlinear operator). (b) Image obtained with IDA. (c) Illustration of operator (4) (coherent nonlinear operator). (d) Image obtained with CDA.

unweighted and weighted (assigning zeros). In this case, the CDA shows a better performance than the incoherent one.

V. CONCLUSION

In this letter, we introduce the linear and nonlinear apodization methods for bistatic SAR imaging aiming at UWB SAR systems, in which the recently introduced $\omega - k$ relationship plays an important role in designing 2-D windows for the apodization methods. The methods allow controlling sidelobe without loss in resolutions. For illustration purposes, we considered IDA and CDA in the simulations. The simulation results show the efficiency of IDA and CDA.

REFERENCES

- [1] M. Soumekh, "Bistatic synthetic aperture radar inversion with application in dynamic object imaging," *IEEE Trans. Signal Process.*, vol. 39, no. 9, pp. 2044–2055, Sep. 1991.
- [2] O. Loffeld, H. Nies, V. Peters, and S. Knedlik, "Models and useful relations for bistatic SAR processing," *IEEE Trans. Geosci. Remote Sens.*, vol. 42, no. 10, pp. 2031–2038, Oct. 2004.
- [3] Y. L. Neo, F. H. Wong, and I. G. Cumming, "Processing of azimuth-invariant bistatic SAR data using the range Doppler algorithm," *IEEE Trans. Geosci. Remote Sens.*, vol. 46, no. 1, pp. 14–21, Dec. 2007.
- [4] R. Baque *et al.*, "LORAMBis a bistatic VHF/UHF SAR experiment for FOPEN," in *Proc. IEEE Radar Conf.*, May 2010, pp. 832–837.
- [5] H. C. Stankwitz, R. J. Dallaire, and J. R. Fienup, "Nonlinear apodization for sidelobe control in SAR imagery," *IEEE Trans. Aerosp. Electron. Syst.*, vol. 31, no. 1, pp. 267–279, Jan. 1995.
- [6] X. Xu and R. M. Narayanan, "Enhanced resolution in SAR/ISAR imaging using iterative sidelobe apodization," *IEEE Trans. Image Process.*, vol. 14, no. 4, pp. 537–547, Apr. 2005.
- [7] C. Cafforio, C. Prati, and F. Rocca, "SAR data focusing using seismic migration techniques," *IEEE Trans. Aerosp. Electron. Syst.*, vol. 27, no. 2, pp. 194–207, Mar. 1991.
- [8] V. T. Vu, "Area resolution for bistatic ultrawideband ultrawide-beam SAR," *IEEE Trans. Aerosp. Electron. Syst.*, vol. 57, no. 2, pp. 1371–1377, Apr. 2021.
- [9] V. T. Vu, T. K. Sjögren, and M. I. Pettersson, "On apodization methods for ultra-wideband SAR imaging," in *Proc. 6th Eur. Radar Conf.*, Rome, Italy, Sep. 2009, pp. 529–532.